



Article

# Increase in Elastic Stress Limits by Plastic Conditioning: Influence of Strain Hardening on Interference Fits

Mario Schierz

Ingenieur-Service Schierz, Skalablick 7, 02708 Loebau, Germany; dr.mario.schierz@ingenieurservice-schierz.de

**Abstract:** This paper presents a novel method for the design of purely elastic interference fits by exploiting the plastic properties of a material. In this process, the elastic potential of the material is expanded by the targeted application of residual stresses and material strengthening, in such a way that additional operational loads due to rotating bending moments, torsion, temperature changes, and centrifugal forces are absorbed by the hub in a purely elastic manner, and plastic deformations are avoided. In the ideal case, the performance shown by the connection can be almost doubled compared to conventional elastically joined interference fits. Compared with conventional elastically-plastically joined interference fits, a specifically defined additional safety against plastic deformation can be guaranteed. In addition to the prerequisites of plasticity theory, the fundamental aspects of the process are presented and investigated on the basis of two-dimensional numerical calculation models. Both ideal plastic and hardening material models were used. The results of this work showed that previous stress limits can be significantly increased up to full plastic loading and that the utilization of plastic material properties is also made possible by plastic conditioning for applications that were previously designed to be purely elastic.

**Keywords:** plastic conditioning; plastically joined interference fits; increase in elastic stress limits; strain hardening of interference fits; plastic behavior of materials; residual stresses; joint pressure; interference fit assembly



**Citation:** Schierz, M. Increase in Elastic Stress Limits by Plastic Conditioning: Influence of Strain Hardening on Interference Fits. *Appl. Mech.* **2022**, *3*, 375–389. <https://doi.org/10.3390/applmech3020023>

Received: 24 February 2022

Accepted: 25 March 2022

Published: 31 March 2022

**Publisher's Note:** MDPI stays neutral with regard to jurisdictional claims in published maps and institutional affiliations.



**Copyright:** © 2022 by the author. Licensee MDPI, Basel, Switzerland. This article is an open access article distributed under the terms and conditions of the Creative Commons Attribution (CC BY) license (<https://creativecommons.org/licenses/by/4.0/>).

## 1. Introduction

In the context of intensified competitive conditions, manufacturers are increasingly focusing on reducing costs and increasing the volume utility value of their products. Important starting points for this, beginning with product development, are savings in labor, energy, and materials. From an ecological point of view, maximizing material utilization is becoming increasingly important. For this reason, scientists and engineers have been working for many decades to extend the stress limits of technical components. The theory of plasticity makes an important contribution to this research. It enabled the computational basis for stressing components beyond their elastic limit, thus making them more efficient without compromising operational safety and structural strength [1].

## 2. Problem Description

Despite their now well-established theoretical foundations, the application of elastically-plastically designed interference fits (PVs) is rather underrepresented in industrial practice; therefore, this often leads to very conservatively designed components. The reasons for this reticence are, on the one hand, the relatively large spreads of the influence parameters; on the other hand, plastic design requires high interference values in the interference fits, which can only be joined thermally to a limited extent. For certain applications, such as oil-jointed interference fits or components in safety-critical systems, the safe avoidance of plastic deformation during operation is technologically mandatory. Another important obstacle to the practical application of elastically-plastically stressed PV has so far been

the additional stresses garnered during operation, in addition to the limited normative design regulations.

The majority of PVs are subjected to dynamic stresses in practice. These primarily result from rotating bending moments and dynamic torques, as well as thermally induced stresses and transient centrifugal forces. Calculation bases and design rules for the production of elastic-plastic interference fits have been in existence for some time [2]. These components are dimensioned in such a way that a plastic state is created during the joining process, in which an additional increase in material stress due to dynamic operating loads inevitably leads to further, usually uncontrolled plastic deformations. When these dynamic loads subside, the interference fit no longer returns to the initial stress state due to these additional plastic deformations. One consequence of this is the loss of joint pressure in the contact zone, which leads to a reduction of transmissible forces and torques, and thus can endanger the operational safety or service life of the components.

There are a number of publications on this subject, in which the loss of joint pressure after the plastic load of interference fits during operation has been investigated in more detail [3–5]. To illustrate these relationships, please refer to the representation of stress states in Figure 1. Here, the ideal plastic stress changes at the inner diameter of an outer part (hub) under internal pressure are shown in the principal stress plane, assuming the plane stress state (ESZ). Their axes are formed by the radial stress on the abscissa and the tangential stresses on the ordinate. The ellipse represents the ideal plastic yield strength according to Equations (2) and (3) (Section 3.2).

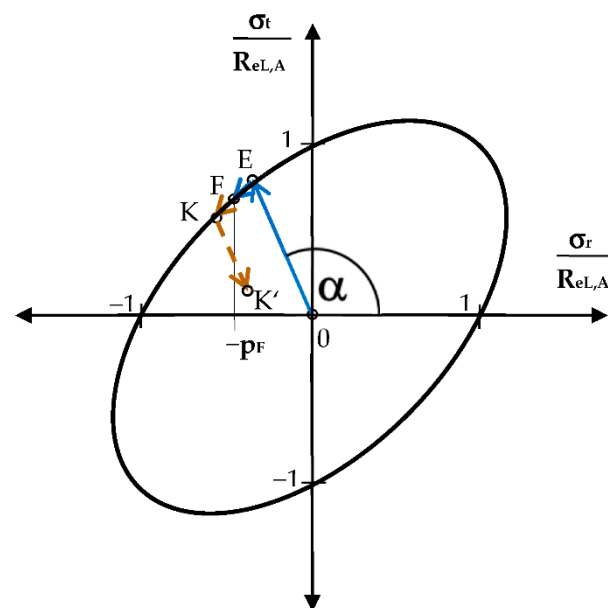


**Figure 1.** Principal stresses at the inner diameter of the outer part of an interference fit with an ideal plastic yield strength (GEH).

In previous practice, elastically–plastically designed interference fits with a joint pressure of  $p_F$  (identical to the negative radial stress  $p_F = -\sigma_r$ ) are produced during the joining process, as shown in Figure 1, along the load path  $\overline{OE} - \overline{EF}$  (blue arrow/solid line).

According to Kollmann [2], the angle of inclination  $\alpha$  of the straight line  $\overline{OE}$  is determined exclusively by the diameter ratio  $Q_A$  of the component, as shown.

$$\sigma_t = -m \cdot \sigma_r \text{ mit } m = \frac{1 + Q_A^2}{1 - Q_A^2} = -\tan(\alpha) = \tan(180^\circ - \alpha) \text{ and } Q_A = \frac{D_{iA}}{D_{aA}} \quad (1)$$

Point F then marks the stress state at the inner diameter of the outer part of the interference fit after the completion of the joining process. Since point F lies on the graph of

yield strength, increases in stress lead to changes in stress along with the yield strength, and thus, inevitably, to further plastic deformations.

In the present example, the stress state moves to point **K** by increasing the radial stress. After this increased stress is relieved, elastic relief takes place along the relief path  $\overline{KK'}$  (brown arrow/dashed), whereby the inclination angle of the straight line of relief, in accordance with Kollmann’s work, is also defined by the diameter ratio  $Q_A$  of the component according to Equation (1), and is, thus, always parallel to the load line. As a result of the plastic deformations, the stress state that develops thereafter must lie in a region to the right of  $-p_F$  along the relief path (for example, at point **K'**). Thus, the previous joint pressure  $p_F$  can no longer be reached due to the loss of plastic interference, which may result in impairments of the operational safety or the service life of the components [6,7]. A description of the points in Figure 1 is as follows:

- E**: Purely elastically joined state at the yield strength;
- F**: Elastically–plastically joined state (conventional according to DIN 7190-1 [8]);
- K**: Stress state on the yield strength with plastic stress increase after joining;
- K'**: State of stress after relief of the plastic stress at point **K**.

### 3. Materials and Methods

#### 3.1. Problem-Solving through the Plastic Conditioning of Interference Fits—Basic Concept of the Procedure

To solve the aforementioned problem, a method was developed for the production of a new generation of interference fits that were designed to be purely elastic, although the plastic potential of the material was exploited to a high degree [6,7]. The basic idea of this method of plastic conditioning was based on the fact that an elastic-plastic pretreatment of the joining partners of an interference fit is carried out before or during the joining process, for example, by applying a conditioning pressure  $p_K$  to a hub (see Figure 2).

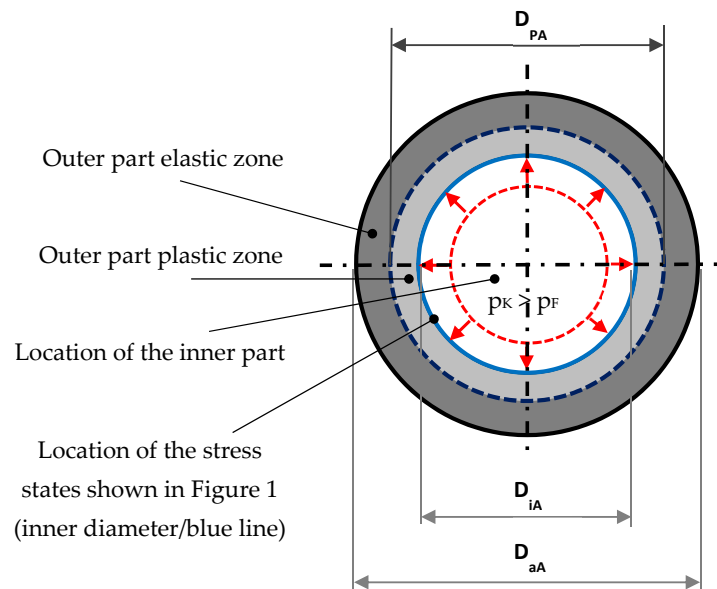


**Figure 2.** Plastic conditioning of a hub by the application of a conditioning pressure,  $p_K$  [6].

This anticipates the process described in Section 2, as shown in Figure 1. During the subsequent elastic relief and, if necessary, subsequent reloading of these joining partners, a purely elastic stress state can be established in such a way that all additional stresses to be expected on the hub during operation lead exclusively to purely elastic stress changes.

In this case, material strain hardening and residual stresses are specifically used in the calculation in such a way that an equal performance to that of conventionally elastically–plastically joined interference fits [8–10] is achieved. However, additional safety against plastic deformations during operation can also be ensured. Compared to conventional

purely elastically designed interference fits [8,11], a significant increase in the joint pressure and, thus, in the transmittable forces and torques, is possible with the same or higher protection against plastic deformations.

The procedure, including its basic components and further detailed explanations, was published in [6]. Here, both the basic physical relationships and possibilities for their practical implementation are presented. The decisive influencing parameters are shown and solution approaches for their application in the engineering practice are described. Further analytical calculation methods with the underlying stress-mechanical relationships and associated formulas were explained in detail in [12].

### 3.2. Analytical Investigations (Two-Dimensional, Ideal Plastic Calculation Example)

In the following section, the analytical calculation methods for the plastic conditioning of interference fits are demonstrated using the example of a hub with  $Q_A = 0.45$  and a yield strength of  $R_{eL,A} = 370 \text{ MPa}$ , followed by an explanation of the numerical calculation methods in Section 3.3; reference is also made to the respective stress states in the principal stress plane (Figure 3). For the sake of clarity, the shaft is not shown here; the following considerations are based on the radial stress at the inner diameter of the hub. This is identical in magnitude to the joint pressure of the joined connection with the shaft and is, thus, a decisive parameter for the transmissible forces and torques. Based on the ductile ideal plastic behavior of materials according to the GEH, the ESZ, and a safety requirement against plastic deformations of  $S_{PA} = 1.5$ , the achievable joint pressures of conventionally purely elastically joined interference fits were compared with those of plastically conditioned ones. The GEH was used here as the equivalent stress hypothesis because it agrees very well with the experimental results obtained in practice for a ductile isotropic material; for this reason, it is of greater importance for engineering practices than SH, which is used primarily to describe the brittle behavior of materials such as gray cast iron. The von Mises yield function (GEH) of the principal stresses is as follows Equation (2):

$$F_{GEH} = \frac{1}{6} [(\sigma_1 - \sigma_2)^2 + (\sigma_2 - \sigma_3)^2 + (\sigma_3 - \sigma_1)^2] - k^2 = 0 \tag{2}$$

This results in yield strength in the form of an ellipse, according to Figure 3 (represented by closed lines), for the plane stress state (ESZ) in the principal stress plane. Accordingly, the equation below can be used to calculate the equivalent stress:

$$\sigma_v^2 = \frac{1}{2} [(\sigma_t - \sigma_r)^2 + (\sigma_r - \sigma_z)^2 + (\sigma_z - \sigma_t)^2] \tag{3}$$

The equivalent limit stress  $\sigma_{v,lim}$  for a yield strength of  $R_{eL,A} = 370 \text{ MPa}$  was calculated with a safety against plastic deformation of  $S_{PA} = 1.5$ , as the quotient of these two, to  $\sigma_{v,lim} = 247 \text{ MPa}$ . According to Equation (4), in compliance with the GEH, a yield pressure of  $p_{N,lim} = 113 \text{ MPa}$  was calculated (see also point  $F_{elast}$  in Figure 3). From Equation (1) in connection with Equation (3) for  $\sigma_z = \sigma_z = 0$ , this was as follows:

$$p_{N,lim} = \sqrt{\frac{\sigma_{v,lim}^2}{m^2 + m + 1}} \tag{4}$$

The difference between joint pressure-related safety against plastic deformation and the equivalent stress-related safety was explained in detail elsewhere for conditioned press joints in [6,12]. The current document assumes an equivalent stress-related safety against plastic deformation ( $S_{PA}$ ). For the current example assuming the ideal plastic behavior of the material, a conditioning pressure  $p_{Kond,max} = -\sigma_r = 311 \text{ MPa}$  was used (point K in Figure 3). After conditioning, this also represented the new load limit  $p_{N,lim}$  for purely elastic joint pressures with a safety against plastic deformation of  $S_{PA} = 1.0$ . Only when this pressure was exceeded at the inner diameter of the hub did further plastic deformation occur.

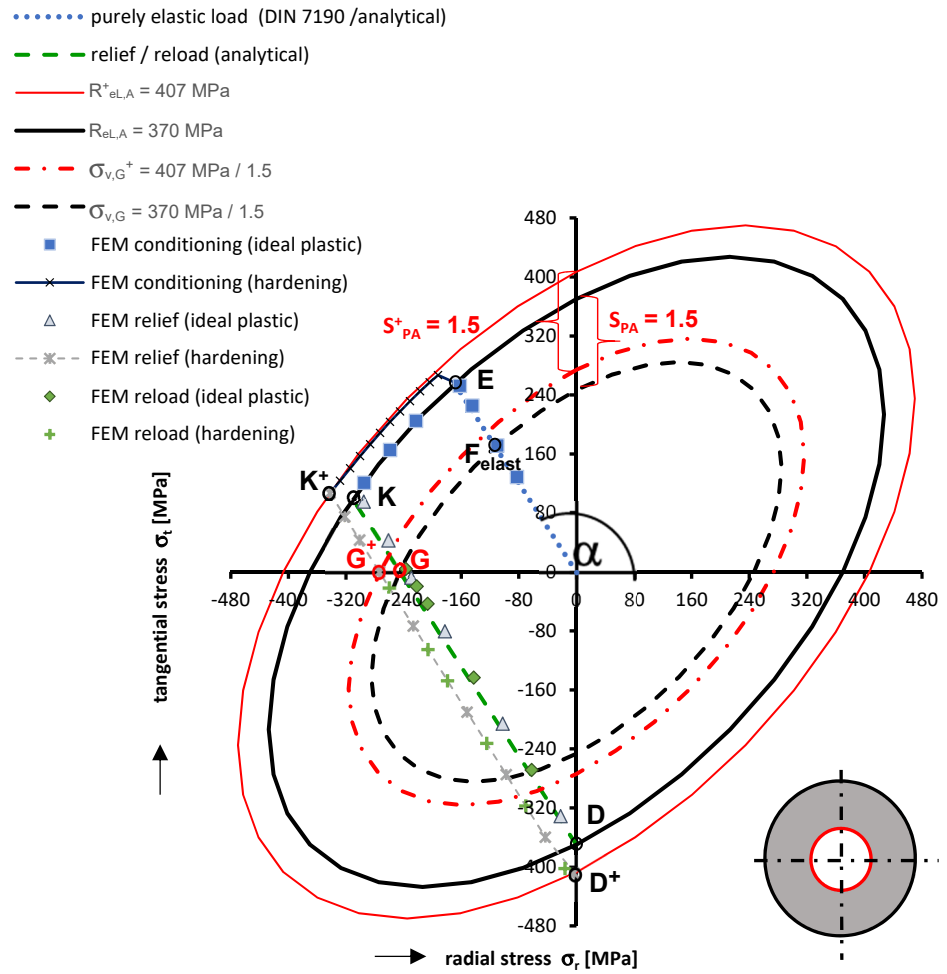


**Figure 3.** Stress states (analytically and numerically determined) at any point of the inner diameter (marked in red) of an outer part with  $Q_A = 0.45$  in the principal stress plane, based on the von Mises yield criterion during conditioning.

The point of intersection of the relief straight line  $\overline{KD}$  with the equivalent stress curve was at  $S_{PA} = 1.5$ , i.e., the searched stress point was located together with point  $F_{elast}$  on the common equivalent stress curve  $\sigma_{v,lim} = 370 \text{ MPa}/1.5$  (shown by the dashed black ellipse in Figure 3), which represents the joint state (point  $G$ ) of the hub after the previous conditioning. The equation for the relief straight line  $\overline{KD}$  in Figure 3 is in Equation (5):

$$y = -m \cdot \sigma_r - \sigma_t = R_{eL,A} \tag{5}$$

where  $y$  marks the intersection of the relief straight line with the ordinate (tangential residual stress after complete relief at point  $D$  in Figure 3). According to Equation (6), the joint pressure of the conditioned interference fit here is  $p_{E,Kond} = -\sigma_r = 246 \text{ MPa}$  (see point  $G$  in Figure 3), which corresponds to an increase in the transmission capacity of the interference fit to 218%.

$$\sigma_v^2 = (m^2 + m + 1) \cdot \sigma_r^2 + (2 \cdot m \cdot y + y) \cdot \sigma_r + y^2 \tag{6}$$

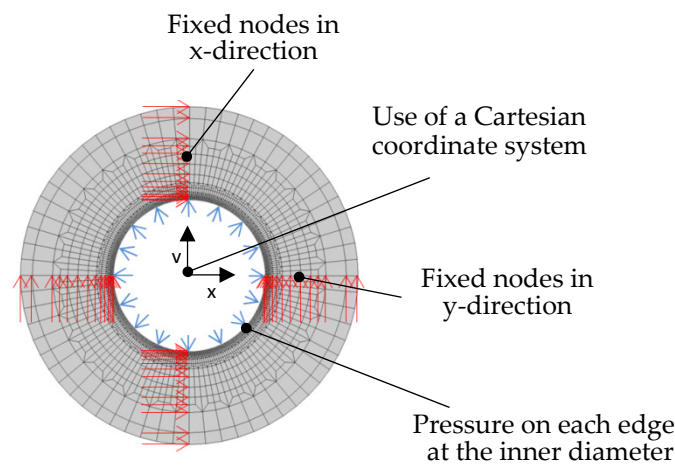
Assuming arbitrary radial stresses on the relief straight line, point  $D$  after complete relief at the end of the conditioning process for the GEH can be calculated as follows:

$$\begin{aligned} D_{\sigma_r(GEH)} &= 0; \\ D_{\sigma_t(GEH)} &= -m \cdot \sigma_r - \left( \frac{\sigma_t}{2} + \sqrt{\left(-\frac{\sigma_r}{2}\right)^2 - (\sigma_r^2 - \sigma_v^2)} \right) \end{aligned} \tag{7}$$

In addition to the enormous potential for increasing the elastic transmission of forces and torques demonstrated by the plastic conditioning method described in this section, for the first time, the theoretical knowledge gained in this respect enables a complete analytical description of the elastic-plastic stress states at the inner diameter of a hub based on the GEH, which until now has been limited to numerical solutions.

3.3. Numerical Verification of the Analytical Investigations (Ideal Plastic)

To verify the test results of the analytical calculation example, the results were checked using a two-dimensional FE(Finite elements) model of an identical hub (see also Scheme 1). The associated data of the numerical model are listed below (Table 1).



Scheme 1. Meshing of the FE model with the boundary conditions and loads.

Table 1. Data of the numerical model.

Geometry Data			
Hub outer diameter	$D_{aA}$	133.33	mm
Hub inner diameter	$D_{iA}$	60.00	mm
Hub diameter ratio	$Q_A$	0.45	-
Hub material			
Designation	C 45		
Yield strength	$R_{eL,A}$	370	MPa (ideal plastic)
Young's modulus	$E_A$	205,000	MPa
Poisson's ratio	$\nu_A$	0.3	-
Technological Data			
Joint pressure for conditioning	$p_{Kond,max}$	311	MPa
Target safety against plastic deformation	$S_{PA}$	1.5	-

Furthermore, Scheme 1 shows the meshing of the FE model, as well as the boundary conditions and loads used. Based on a Cartesian coordinate system, all nodes were fixed along the abscissa in the  $y$ -direction and along the ordinate in the  $x$ -direction (red arrows in Scheme 1).

The load was defined as the pressure on each edge of an element (2D elements) at the inner diameter of the outer part. In Scheme 1, this is only symbolically represented by the blue arrows, since the edge lengths of the elements in this area, which are important for calculation, are smaller than 0.4 mm.

The FE model was calculated using different FEM systems, the results of which all showed good consistency.

The individual work steps of the numerical investigations are explained in more detail below.

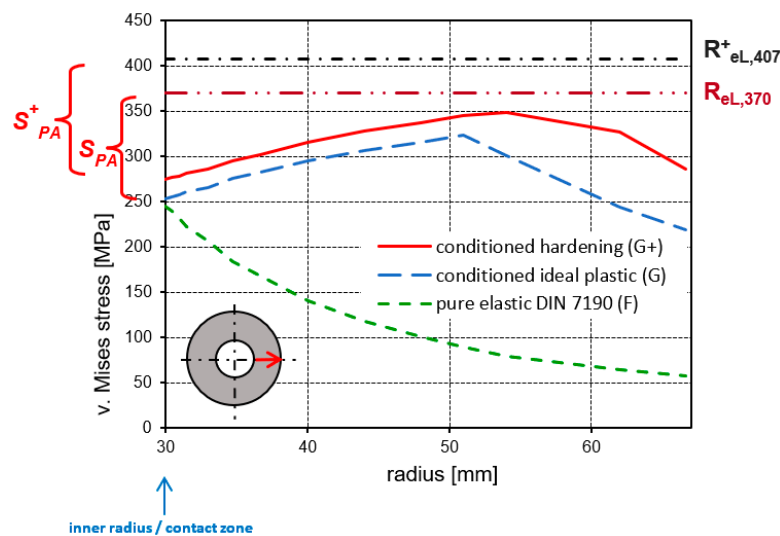
An internal pressure  $p_i$ , as shown in Figure 2, was applied as a load. This was gradually increased up to the conditioning pressure  $p_{Kond,max} = 311 \text{ MPa}$  (point K in Figure 3), and then gradually reduced again to 0 (point D). This was followed by reloading up to  $p_{E,Kond} = 246 \text{ MPa}$  (point G) according to the load history analogous to Figure 3. The load steps examined for comparison are listed in Table 2.

**Table 2.** Load steps of the load history of the ideal plastic behavior of a material, according to Figure 3.

Load Step	$p_i/\text{MPa}$
1 ( $F_{elast}$ )	113
2 (K)	311
3 (D)	0
4 (G)	246

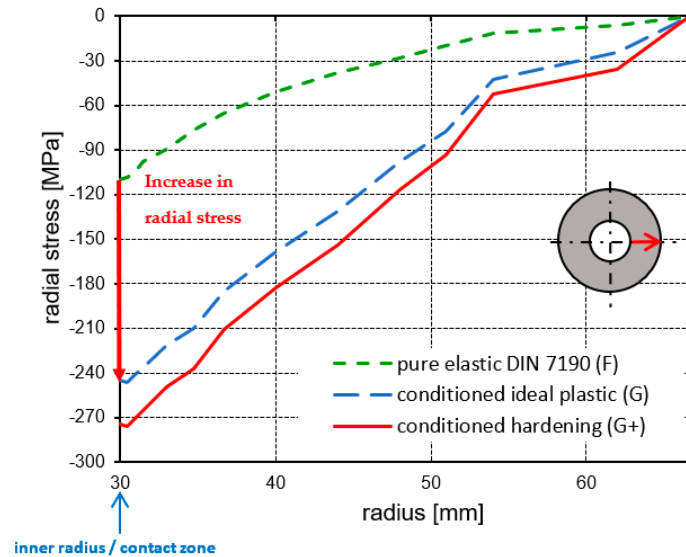
The following illustrations show the graphs of the principal stresses along the radial evaluation path over the complete cross-section of the hub (see red arrow in the diagram sketch) as a function of the applied internal pressure  $p_i$  for load steps 1 and 4. These allow comparison of the stresses in the hub for a conventionally purely elastically joined interference fit according to DIN 7190-1 (pure elastic DIN 7190 ( $F_{elast}$ )) and a plastically conditioned one (conditioned ideal plastic (G)). For reasons of better clarity in direct comparison, the calculation results for the conditioned hardening material (conditioned hardening ( $G^+$ )), which is described in more detail in Section 3.4, are presented as well. The values of the graphs at the radius coordinate of 30 mm show the stress state of the respective load steps at the inner diameter of the hub for the different joining states and are thus directly comparable with the analytical results shown in Figure 3.

Figure 4 represents the von Mises stress in the assembled state (for each of the points  $F_{elast}$ , G, and  $G^+$ ), with a safety against plastic deformation of the outer part  $S_{PA} = 1.5 = S^+_{PA}$  ( $S^+_{PA} \rightarrow$  after hardening of the material) based on a yield strength  $R_{eL,A} = 370 \text{ MPa}$ . The values for the points  $F_{elast}$  ( $\sigma_v = 245 \text{ MPa}$ ) and G ( $\sigma_v = 253 \text{ MPa}$ ) only differed by the numerical deviations and were in good approximation to the analytical specifications.



**Figure 4.** Von Mises stresses in the stress states of points  $F_{elast}$ , G, and  $G^+$  with a safety against the plastic deformation of the outer part  $S_{PA} = 1.5 = S^+_{PA}$  ( $S^+_{PA} \rightarrow$  after hardening of the material).

In Figure 5, the radial stresses for points  $F_{elast}$ ,  $G$ , and  $G^+$  are shown, which are identical to the magnitude of the joint pressure ( $p_F = -\sigma_r = p_i$ ) at the radius coordinate at 30 mm.



**Figure 5.** Radial stresses in the stress states of the points  $F_{elast}$ ,  $G$ , and  $G^+$  with a safety against plastic deformation of the outer part  $S_{pA} = 1.5 = S^+_{pA}$  ( $S^+_{pA} \rightarrow$  after hardening of the material).

This is a technologically significant quantity for the transmission of forces and torques between the shaft and hub. At point  $F_{elast}$  (purely elastically joined state, according to DIN 7190-1), this is  $\sigma_r = -110$  MPa and at point  $G$   $\sigma_r = -245$  MPa. When comparing the two, it is clear that the conditioned hub has a significantly higher value of radial stress for transmitting forces and torques, while the hub maintains the same level of safety against plastic deformations as in a conventionally joined purely elastic state, according to DIN 7190-1.

The low tangential stresses of the inner diameter of the conditioned hub (point  $G$  in Figure 6) correspond to those in Figure 3 and illustrate the residual stresses caused by plastic conditioning. In contrast, the tangential stress at point  $F_{elast}$  of the inner diameter of the hub is  $\sigma_t = 171$  MPa.

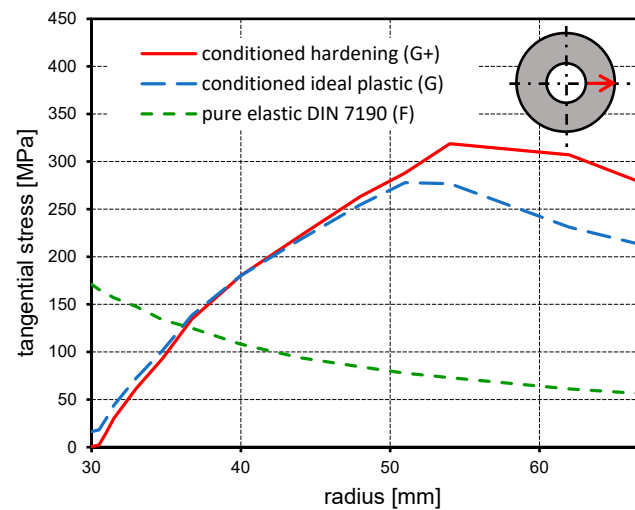


**Figure 6.** Tangential stresses in the stress states of the points  $F_{elast}$ ,  $G$ , and  $G^+$  with a safety against plastic deformation of the outer part  $S_{pA} = 1.5 = S^+_{pA}$  ( $S^+_{pA} \rightarrow$  after hardening of the material).

Overall, the values obtained by means of the FEM in this section showed very good congruence with the analytical calculation results from Section 3.2. In the following paragraphs, the stress graphics (hub quarter section) of the equivalent stress according to the GEH of the FE model for points K, G, and D are also presented. Because of the relatively large differences in the stress gradients, the partial images in Figure 7 were each given their own scale for better graphical resolution of the stress values.

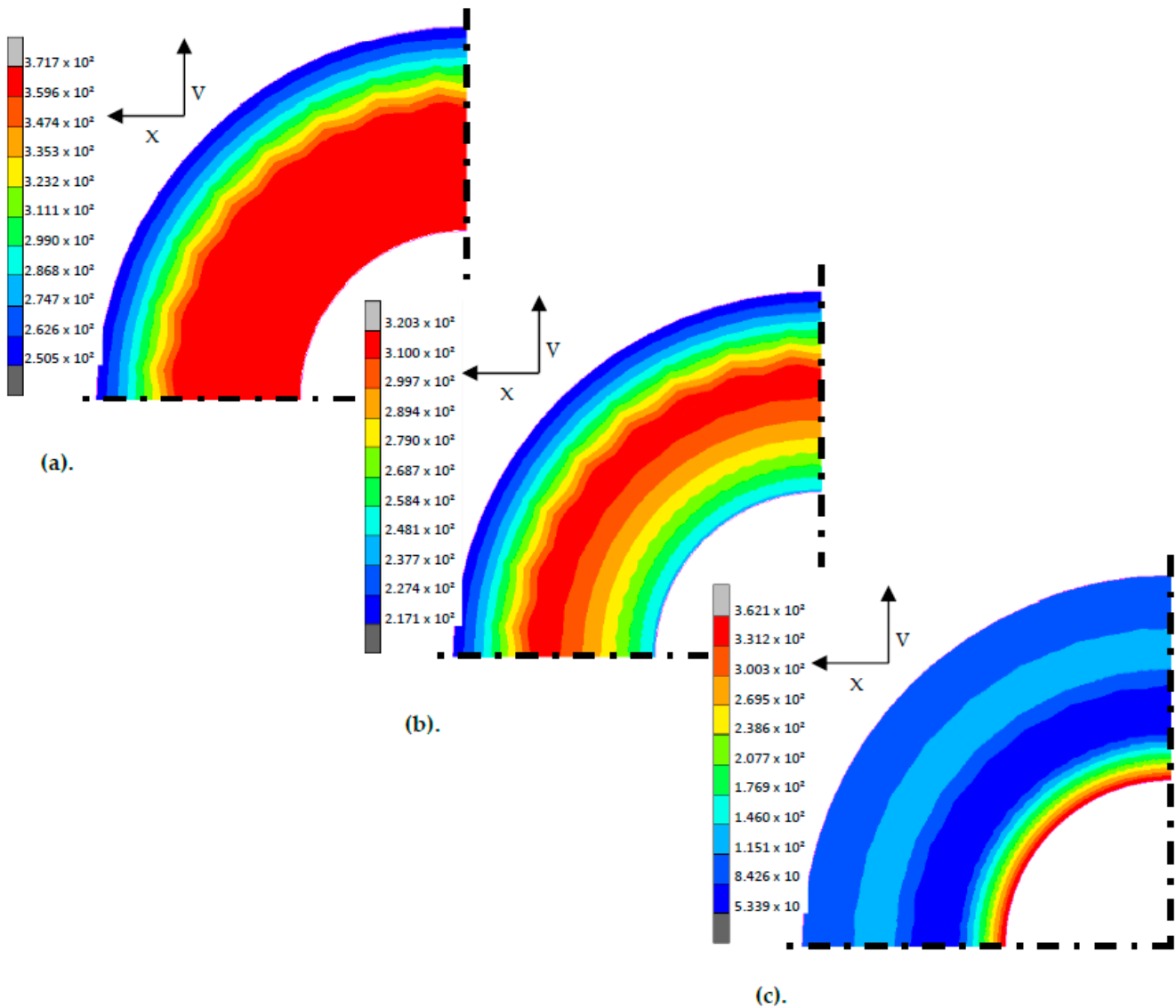


Figure 7. FE stress graphics (hub quarter section) of the equivalent stresses (GEH) for the load points K, G, and D [12]. (a)  $\sigma_v$  at point K; (b)  $\sigma_v$  at point G; (c)  $\sigma_v$  at point D.

The deviations of the lines of identical stress from the circular shape in the outer area of the hub were due to numerical divergences caused by the shape of their meshing. However, according to the principle identified by Saint-Venant, these divergences diminish with increasing distance from the point of origin, so that in the area of the inner diameter of the hub to be investigated, due to sufficiently fine meshing, **very good agreement can be seen in the results of the numerical calculations with the analytical results shown in Figure 3.**

For the analytical calculation of elastic-plastic stress conditions of the inner diameter of the hub on the basis of GEH, a series of formulas specially developed for this purpose are presented for the first time in Section 3. This means that analytical investigations are

now possible in areas that were previously the exclusive domain of numerical methods. In the particularly interesting sector defined by the relief's straight lines, the corresponding stress points from the individual load steps of the FE calculation are plotted in Figure 3. Here, too, the analytical calculation results were validated by their very good agreement with the numerical results.

### 3.4. The Influence of Strain-Hardening

During the plastic stress (e.g., conditioning) of a hardening material, its yield strength is increased from  $\sigma_0$  to  $\sigma_{n2}$  (Figure 8). After a subsequent purely elastic relief to  $\sigma_{n3}$  in Figure 8, renewed reloads between  $\sigma_{n3}$  and  $\sigma_{n2}$  were also purely elastic. New plastic stresses only occurred when the previous stress level  $\sigma_{n2}$  was exceeded. Thus, at point  $\sigma_{n4}$ , the same safety against plastic stress  $S_P$  was achieved as with the stress state  $\sigma_x$  (without conditioning), but at a significantly higher stress level.

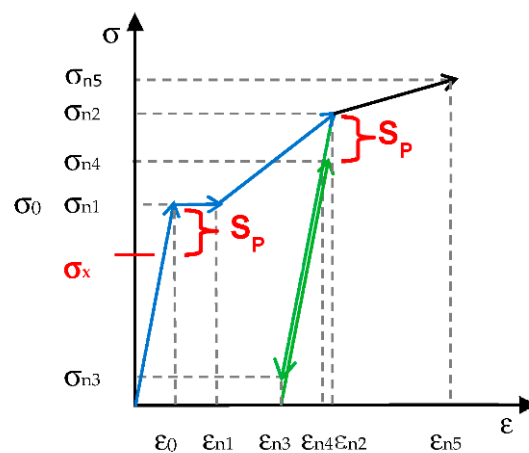


Figure 8. Example of strain hardening (multilinear) [12].

This relationship presents an analogy with the effect of residual stresses described above; it explains the additional increase potential when material strain hardening is taken into account, compared to the ideal plastic behavior of a material. The computational proof of this finding has already been presented in Figures 4–6 in the previous section.

For this purpose, numerical investigations based on hardening material properties were carried out using the FE model presented earlier. The material data for these investigations were taken from a tensile test for C 45 conducted by the IKAT of Chemnitz University of Technology and are listed in Table 3.

Table 3. Data from the tensile test for C45 (IKAT).

$\sigma_v$ (MPa)	$\epsilon_v$ (-)
370.00	0.00171
390.00	0.00182
400.00	0.00189
410.00	0.01303
420.00	0.01417
430.00	0.01549
440.00	0.01665
470.00	0.02075

**Table 3.** *Cont.*

$\sigma_v$	$\varepsilon_v$
500.00	0.02543
530.00	0.03097
560.00	0.03775
590.00	0.04612
620.00	0.05967

The FE calculation procedure was analogous to that for the ideal plastic behavior of a material but with modified internal pressure  $p_i$ . The changed values of the individual steps are shown in Table 4 and are explained in more detail below.

**Table 4.** Load steps of the load history with hardening of the material, according to Figure 3.

Load Step	$p_i$ /MPa
1 ( $F_{\text{elast}}$ )	113
2 ( $K^+$ )	342
3 ( $D^+$ )	0
4 ( $G^+$ )	274

An internal pressure of  $p_i$  according to Figure 2 was applied as the load. This was gradually increased up to the conditioning pressure, which in this experiment was  $p_{K_{\text{ond,max}}} = 342 \text{ MPa}$  (point  $K^+$  in Figure 3). In contrast to the ideal plastic material, the equivalent stress here increased to  $\sigma_v = 407 \text{ MPa}$ , due to the strain hardening of the material.

#### 4. Discussion of the Results of the FE Calculations with Hardening Material and Comparison with Ideal Plastic Investigations

The path for the change of the respective stress states during the load increase is represented in Figure 3 by the black -x-x-x-x- line. The gradient of the stress change in the respective load step is mainly defined by the stress-strain curve (represented by the blue dashed line in Figure 9), which is determined by the values found in Table 3. The stress range applied during the FE calculation is represented on the stress-strain curve with a red dashed line.

In the subsequent purely elastic step-by-step relief up to  $p_i = 0 \text{ MPa}$  (point  $D^+$ ), this equivalent stress then marks the new amount of the yield strength (represented by the black dash-dot line in Figures 4 and 9 and also by the red ellipse in Figure 3). Each reload is then made purely elastic up to this value. Only if this new yield strength is exceeded will further plastic deformations occur.

This consideration is then inevitably followed by a new equivalent limit stress  $\sigma_{v,\text{lim}}^+$  for the predetermined safety against plastic deformation of  $S_{PA} = 1.5$  with  $\sigma_{v,\text{lim}}^+ = 274 \text{ MPa}$  (represented by the red line-point ellipse in Figure 3). Their point of intersection with the load straight line  $\overline{D^+K^+}$  indicates point  $G^+$  for the desired stress state, with  $p_{E,K_{\text{ond}}} = 274 \text{ MPa}$ . The identity of the aforementioned equivalent limit stress shows that the tangential stresses disappear here.

With  $\sigma_v = 274 \text{ MPa}$ , the equivalent stress at point  $G^+$  (Figure 4) is greater than that for the ideal plastic material ( $\sigma_v = 253 \text{ MPa}$  at point  $G$ ), where the yield strength  $R_{eL,A}^+$  (black line-point line in Figure 4) has also increased as a result of the material strain hardening. The identity of the safety against the plastic deformation of  $S_{PA} = 1.5 = S_{PA}^+$  ( $S_{PA}^+ \rightarrow$  after hardening of the material) was a prerequisite for the comparability of the investigated modes and a central point of the task (see Section 3.2). However, for the sake of clarity, the

safety shown in Figures 3 and 4 was symbolized as differences between  $R_{eL,A}$  and  $\sigma_{v,lim}$  or  $R_{eL,A}^+$  and  $\sigma_{v,lim}^+$ . Therefore,  $S_{pA}$  at this point appears to be lower than  $S_{pA}^+$  due to the smaller amounts of  $R_{eL,A}$  and  $\sigma_{v,lim}$ . The values for radial stress are shown in Figure 5 (represented by the red line), which illustrates their additional reinforcement compared with the ideal plastic material (represented by the blue dashed line).

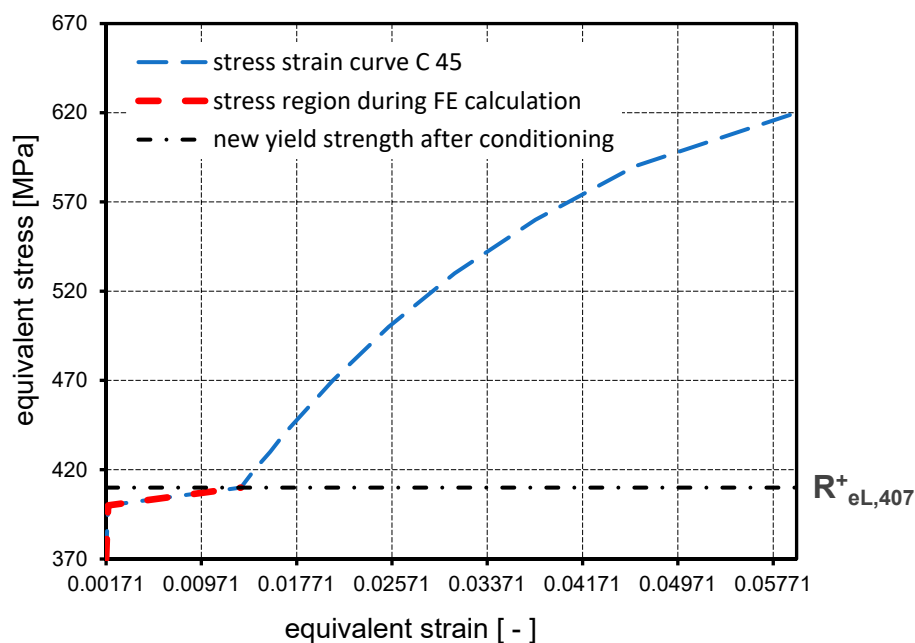


Figure 9. Stress–strain curve of the tensile test from IKAT.

## 5. Conclusions Regarding Engineering Practice and Industrial Applications

For joint pressure as a technological target value, these investigations revealed a potential for an increase of up to 243% with the **plastic conditioning method**, compared to conventional elastically joined interference fits, taking into account the material's strain hardening. With the ideal plastic behavior of the material, this increase in potential was 218%. In addition to the residual stresses mentioned in Section 3.3, the elastic potential of the component is additionally increased by hardening during the conditioning, which means that higher joint pressures for the transmission of forces and torques can be realized in engineering practice.

The plastic conditioning process can increase the load limits of the components while saving installation space, weight, material quantity, and labor. Because of the high interferences required, the process is particularly suitable for longitudinal press-fit joints. In the case of conical interference fits, however, conditioning can be integrated into the joining process and, thus, does not involve any additional manufacturing effort. This is especially true in the case of oil press-fit joints, where the process makes the plastic potential usable in the first place. However, the process is also of interest for cylindrical interference fits because part of the required interference is already introduced by the plastic deformation during conditioning and the setting losses are also already realized in this context, which is particularly important for smaller joint diameters. The additional effort involved is manageable since it relates to only one additional manufacturing step. Commercially available clamping elements, for example, can be used as tools. When using cone clamping elements, as shown in Figure 10 (RINGSPANN GmbH), the conditioning process can also be integrated into the assembly process.



**Figure 10.** Shaft–hub connection with a cone clamping element (hub clamped on the inside) from RINGSPANN GmbH (Image source: RINGSPANN GmbH).

In addition, it is conceivable that technological processing steps, such as hardening/tempering or grinding, can be omitted since material strain hardening or smoothing processes on the surface already take place during conditioning.

The plastic conditioning process also has high application potential with regard to the dismantlability of press joints.

## 6. Summary and Outlook

The aim of this paper is to present a novel method for the plastic conditioning of interference fits, which for the first time enables the purely elastic design of this machine element using the plastic potentialities of the material used. The results presented here showed that, compared to state-of-the-art conventional methods, significantly higher joint pressures can be achieved with this method of conditioning with the same degree of safety against plastic stress or, with identical joint pressure, greater safety against plastic deformation. The transmissible forces and torques were almost doubled and the resulting equivalent stresses were reduced by more than 30%.

This allows the elastic-plastic design to be controlled in such a way that all operational additional loads can be absorbed purely elastically so that they do not cause any plastic deformations of the joined interference fits. The potential for improvement increases with the decreasing diameter ratio of the components and the increasing material strain hardening.

In addition, this process allows the plastic properties of the material to be used for applications that previously required a purely elastic design with prescribed safety measures against incipient plasticization.

Since the current standardization does not provide for a computational check of the interference fits for plastic stresses during operation, the new method can also largely avoid endangered components that are not recorded in the calculation. In addition, the plastic displacements introduced during conditioning reduce the high joining temperatures that are required for thermally joined interference fits with high interference values.

This work does not claim to offer a conclusive description of the technological process instructions but is rather a conceptualization of the physical principles of action for increasing the performance and effectiveness of a frequently used machine element.

The previous investigations were of a purely theoretical nature, based on analytical and numerical calculations. Current research projects at the IKTD of the University of Stuttgart [13] and IKAT of the Chemnitz University of Technology [14] are also concerned with experimental analyses of plastically stressed interference fits. These projects will make it possible to plan further steps in order to test the existing theoretical findings and to qualify industrial technologies for their application. In addition, three-dimensional FE calculations with a joined shaft are required in order to estimate the deviations in the edge area of the hub from the previously considered plane stress state. Unwanted edge effects occur, especially during rotating bending and joining longitudinally, which could be reduced by plastic conditioning.

Other interesting questions for future research topics concern the influence of plastic conditioning on the fatigue strength of interference fits and its application for internal- high-pressure-assembled press fits, respectively, with transverse impact extrusion assembled press fits with plastically stressed hubs.

## 7. Patents

The newly developed method described in this paper for the **plastic conditioning of interference fits** in drive technology, which forms the basis for the results presented here, was published in the patent specification **DE 10 2016 004 223 B3**. This also contains further details for practical applications and engineering implementation. In addition, the basic physical relationships and decisive influencing parameters are shown.

**Funding:** This research received no external funding.

**Institutional Review Board Statement:** The study did not require ethical approval.

**Conflicts of Interest:** The author declares that there is no conflict of interest.

## Abbreviations

Abbreviation	Unit	Meaning
$d$	mm	Diameter coordinate (control variable)
$D_{aA}$	mm	Outer diameter of the outer part
$D_F$	mm	Joint diameter (nominal)
$D_{iA}$	mm	Inner diameter of the outer part
$D_{PA}$	mm	Plasticity diameter of the outer part
$D_{\sigma r(GEH)}, D_{\sigma t(GEH)}$	MPa	Stress values at point D in the principal stress plane for von Mises yield criterion (GEH)
$E_A$	MPa	Young's modulus of the outer part
$F_{GEH}$	MPa	Von Mises yield function
$k$	MPa	Critical value (yield strength in shear)
$m$	-	Factor for determining the angle of inclination
$p_i$	MPa	Internal pressure of the disc
$p_E$	MPa	Elastic joint pressure at the yield strength
$p_{E, Kond}$	MPa	Elastic joint pressure after previous conditioning
$p_F$	MPa	Joint pressure
$p_K$	MPa	Conditioning pressure
$p_{Kond, max}$	MPa	Maximum joint pressure when undergoing conditioning
$p_{N, lim}$	MPa	Yield pressure (elastic limit) of an outer part
$Q_A$	-	Diameter ratio of the outer part
$R_{eL, A}$	MPa	Lower yield strength of the outer part
$R_{eL, A}^+$	MPa	Lower yield strength of the outer part after hardening
$r$	mm	Radius
$S_P$	-	Safety against plastic deformation
$S_{PA}$	-	Safety against plastic deformation of the outer part
$S_{PA}^+$	-	Safety against plastic deformation of the outer part after hardening
$y$	MPa	Intersection of the relief straight line with the ordinate (tangential residual stress after complete relief)
$\alpha$	°	Inclination angle for load line and relief straight line
$\varepsilon_v$	-	Equivalent strain
$\nu_A$	-	Poisson's ratio of the outer part
$\sigma_r$	MPa	Radial stress
$\sigma_t$	MPa	Tangential stress
$\sigma_v$	MPa	Equivalent stress
$\sigma_{v, G}$	MPa	Equivalent stress at point G

$\sigma_{v,G^+}$	MPa	Equivalent stress at point G <sup>+</sup>
$\sigma_{v,lim}$	MPa	Equivalent limit stress
$\sigma_{v,lim}^+$	MPa	Equivalent limit stress after hardening of the material
$\sigma_1, \sigma_2, \sigma_3$	MPa	Principal stresses of the stress tensor
<b>AT</b>		Outer part of the PV
<b>ESZ</b>		Plane stress state
<b>FE</b>		Finite elements
<b>FEM</b>		Finite element method
<b>GEH</b>		Von Mises yield criterion
<b>PV</b>		Interference fit
<b>MPV</b>		Multiple interference fit
<b>SH</b>		Shear stress hypothesis according to TRESCA
<b>IKAT</b>		Institute of Construction and Drive Technology (TU Chemnitz)
<b>IKTD</b>		Institute for Engineering Design and Industrial Design (University of Stuttgart)

## References

1. Kollmann, F.G. Die Auslegung elastisch-plastisch beanspruchter Querpressverbände. *Forsch. Ing.* **1978**, *44*, 1–11. [[CrossRef](#)]
2. Kollmann, F.-G. *Welle-Nabe-Verbindungen. Konstruktionsbücher, Band 32*; Springer: Berlin/Heidelberg, Germany; New York, NY, USA; Tokyo, Japan, 1984.
3. Leidich, E.; Lätzer, M. *FVA-Nr. 566 I-Heft 993-Übertragungsfähigkeit von Klemmverbindungen Unter Besonderer Berücksichtigung Plastischer Verformungen*; Abschlussbericht, Forschungsvereinigung Antriebstechnik e.V.: Frankfurt, Germany, 2011.
4. Kovács, Á. Thermal stresses in a shrink fit due to an inhomogeneous temperature distribution. *Acta Mech.* **1994**, *105*, 173–187. [[CrossRef](#)]
5. Mack, W. Spannungen im thermisch gefügten elastisch-plastischen Querpreßverband mit elastischer Entlastung. *Ing.-Arch.* **1986**, *56*, 301–313. [[CrossRef](#)]
6. Schierz, M. Steigerung des Elastischen Potenzials von Pressverbindungen Durch Plastische Konditionierung der Fügepartner. Ph.D. Thesis, Technische Universität Chemnitz, Chemnitz, Germany, 2018.
7. Schierz, M.; Leidich, E.; Ziaei, M. Plastisch konditionierte Pressverbindungen. In *VDI (Hrsg) Welle-Nabe-Verbindungen*; VDI-Berichte Nr.: 2018; VDI Verlag GmbH: Düsseldorf, Germany, 2018; Volume 2337, pp. 73–84.
8. *DIN 7190-1:2017*; Pressverbände—Teil 1: Berechnungsgrundlagen und Gestaltungsregeln. DIN Deutsches Institut für Normung e.V.: Berlin, Germany, 2017.
9. Schierz, M.; Leidich, E. *FVA- Nr. 424 II—Heft 871-Erweiterung des Berechnungsprogramms PressFit®*; Abschlussbericht, Forschungsvereinigung Antriebstechnik e.V.: Frankfurt, Germany, 2008.
10. Schierz, M. *FVA- Nr. 424 III—Heft 1170- Erweiterung des Berechnungsprogramms PressFit® für Elastisch und Elastisch-Plastisch Beanspruchte Mehrfachpressoerbände (MPV)*; Abschlussbericht, Forschungsvereinigung Antriebstechnik e.V.: Frankfurt, Germany, 2015.
11. *DIN 7190-2:2017*; Pressverbände—Teil 2: Berechnungsgrundlagen und Gestaltungsregeln für Kegelige, Selbsthemmende Pressverbände. DIN Deutsches Institut für Normung e.V.: Berlin, Germany, 2017.
12. Schierz, M. Plastische Konditionierung von Pressverbindungen in der Antriebstechnik—Ein Verfahren mit Potenzial. *Forsch. Ing.* **2020**, *84*, 345–355. [[CrossRef](#)]
13. Ulrich, D.; Binz, H. Elastisch-plastische Auslegung: Untersuchung von Pressverbindungen mit hohen Übermaßen. In *VDI (Hrsg) Welle-Nabe-Verbindungen*; VDI-Berichte Nr.: 2018; VDI Verlag GmbH: Düsseldorf, Germany, 2018; Volume 2337, pp. 279–282.
14. Günther, C.; Leidich, E.; Hasse, A. Untersuchung der Gestaltfestigkeit hochbeanspruchter Hohlwellen-Pressverbindungen. In *Proceedings of the Dresdner Maschinenelemente Kolloquium, Dresden, Germany, 26–27 December 2019*; Sierke Verlag: Göttingen, Germany, 2019; pp. 381–392.